energies

MDPI

Article

Thermal-Management Performance of Phase-Change Material on PV Modules in Different Climate Zones

Liang Tang [1], Yong Luo [1], Linlin Yin [1], Jinwei Li [2] and Xiaoling Cao [2,*]

[1] Shandong Electric Power Engineering Consulting Corp., Ltd., Jinan 250013, China
[2] School of Mechanical Engineering, Southwest Jiaotong University, Chengdu 610031, China
* Correspondence: xlcao@swjtu.edu.cn

Abstract: Phase-change material (PCM) can enhance the efficiency of photovoltaic (PV) modules by reducing their temperature and is widely studied for thermal management. However, their performance varies due to differences in local solar radiation and climate conditions. Previous studies have mainly focused on the thermal properties of PCM, but practical evaluation should consider specific local conditions. To investigate the thermal-management performance of PCMs in different zones and obtain optimal design parameters, this study investigated the temperature-control effect of PCMs on PV systems across different regions through experiments. The results revealed that the temperature-control performance of PCM was limited in cold regions. Furthermore, the study developed a PCM-PV model and employed response surface methodology along with an NSGA-II to analyze the temperature-control effectiveness of the PCM-PV system in nine regions of China. Pareto solutions were obtained for nine regions in China, balancing annual power generation and system costs. PCM effectiveness is limited in colder regions like Naqu, where it increases power generation by only 0.5%, while in other regions, it improves annual power generation by 1.4% to 3%, especially in areas with high temperatures and abundant solar resources. However, when considering life-cycle gains and initial investment, PCM technology may not always be economically efficient, highlighting the need for region-specific evaluations.

Keywords: phase-change material; photovoltaic; thermal management; multi-objective optimization; power generation

check for updates

Citation: Tang, L.; Luo, Y.; Yin, L.; Li, J.; Cao, X. Thermal-Management Performance of Phase-Change Material on PV Modules in Different Climate Zones. *Energies* **2024**, *17*, 6200. https://doi.org/10.3390/en17236200

Received: 28 October 2024
Revised: 2 December 2024
Accepted: 5 December 2024
Published: 9 December 2024

Copyright: © 2024 by the authors. Licensee MDPI, Basel, Switzerland. This article is an open access article distributed under the terms and conditions of the Creative Commons Attribution (CC BY) license (https://creativecommons.org/licenses/by/4.0/).

1. Introduction

Energy consumption-related environmental issues, particularly those caused by fossil fuels, have gained increasing attention due to their contribution to the greenhouse effect [1]. With technological advancements, renewable energy sources like solar, wind, and geothermal are being increasingly integrated into various applications. Solar energy, in particular, is widely used for its ability to generate both thermal and electrical power. Studies have shown that by 2050, electricity will account for over 50% of final energy consumption, with 90% of the electricity provided by renewable energy sources, and PV power generation will be one of its most essential components [2]. In fact, in 2019, the global installed capacity of PV power reached 578,553 MW [3], and by 2022, it reached 1,046,614 MW [4]. To significantly reduce global greenhouse gas emissions, the installed capacity of PV power generation needs to reach 14,000 GW by 2050 [2]. Therefore, PV power generation has received increasing attention.

PV power generation relies on PV panels that absorb solar energy and convert it into electricity through the "photoelectric" effect [5]. However, most of the absorbed solar energy is converted into heat, causing the temperature of the PV modules to rise and reducing their power generation capacity [6]. To address this issue, many PV thermal-management methods have been proposed, mainly divided into active and passive thermal-management. Active thermal management increases the heat dissipation of PV modules by providing

additional energy to drive cooling media (such as water and air), lowering the temperature of PV panels, and enhancing efficiency [7]. For example, the study has shown that by driving air behind the surface of PV panels, the temperature of PV components can be reduced, and the PV efficiency can be increased from 8.6% to 12.5% [8]. Further study results have demonstrated that actively cooled PV modules have shown a considerable improvement in both PV efficiency and energy efficiency ratio as compared to uncooled PV modules [9]. However, the energy input required for active cooling may increase system energy consumption and costs [10]. In contrast, passive thermal management, which does not require additional energy input, has gained more attention [11]. Among them, PCM which absorb and release heat as they melt and solidify, are considered effective for passive thermal management and energy storage [12].

Numerous studies have explored the use of PCM for thermal management of PV modules. Tan et al. [13] demonstrated that using PCM (RT27) increased the photoelectric efficiency of PV modules by 5.39% compared to systems without temperature control. Stropnik et al. [14] found that using PCM (RT28HC) reduced the temperature of PV modules by 35.6 °C during the day, based on experimental and simulation results. In long-term studies, Hasan et al. [15] showed that PCM improved the annual electricity generation of PV modules by 5.9% in hot climates. Díaz et al. [16] applied a 40 mm layer of $CaCl_2$-$6H_2O$ as PCM, resulting in a 5.8% and 4.5% increase in annual electricity generation in Vicuña and Calama, respectively. These findings highlight the significant impact of PCM on reducing module temperature and improving power generation efficiency.

The ability of PCM to regulate the temperature of PV modules is due to their latent heat during phase change. Different PCMs have varying phase-change temperatures and latent heat of fusion [17]. Some studies suggest that lower phase-change temperatures improve PV module performance [18]. Research indicates that the optimal cooling effect occurs when the phase-change temperature is between 18 and 25 °C [19]. However, if the phase-change temperature is below 25 °C, the PCM may melt too quickly in summer, losing its cooling effect, and may not solidify fully at night, reducing its effectiveness the following day [20]. Other studies show that PCMs with a melting point of 29.8 °C provide better performance improvements than those with a melting point of 22.5 °C [21]. These findings highlight the importance of selecting a PCM with an appropriate phase-change temperature for effective temperature control.

PCMs are typically attached to the back of PV modules, with heat transfer occurring through conduction. The thermal conductivity of the PCM directly impacts its ability to store and release heat. When the PCM melts, it creates additional thermal resistance, which can reduce the heat dissipation from the module [22]. Organic PCMs, commonly used for thermal management, often have low thermal conductivity [23], leading to slow heat storage and release in practical applications [24]. To address this issue, two main approaches are used. One is to enhance heat transfer from the PV module by adding fins or heat pipes. For example, Khanna et al. [25] increased thermal conductivity by adding metal fins, improving conversion efficiency. Gad et al. [26] further reduced the PV module temperature by integrating heat pipes, resulting in a significant efficiency boost. Another approach is to improve the thermal conductivity of PCMs themselves. Das et al. [27] increased the thermal conductivity of PCM (OM35) by 1.66 times by adding 5 wt% aluminum powder, leading to an 18.4% increase in power output. Similarly, Karthikeyan et al. [28] and Asefi et al. [29] showed that increasing PCM thermal conductivity enhances PV module efficiency. One standard method to increase PCM conductivity is by incorporating high-thermal-conductivity materials, such as metal foam [30], expanded graphite [31], and nanoparticles [32]. For instance, Wang et al. [33] combined paraffin with foam copper, significantly improving conductivity compared to pure paraffin. Ling et al. [34] created a composite material by adding 25 wt% expanded graphite (EG) to RT44HC, with conductivity ranging from 4.3 to 10.7 W/(m·K) under different conditions. Harish et al. [35] improved lauric acid PCM conductivity by 230% by adding graphene nanosheets. Sari et al. [36] found a linear relationship between paraffin and expanded graphite conductivity when

the graphite content was below 10wt%. Afaynou et al. [37] compared metal soaking and nanoparticles for improving thermal conductivity. Furthermore, mathematical formulas for calculating the effective thermal conductivity of composite PCMs have been developed [38], and Zhang et al. [39] experimentally verified these formulas, finding they worked well when the graphite content was below 20%.

In addition, the thickness of PCM significantly influences the thermal conductivity of PV module backsides [40]. Ho et al. [41] used numerical simulations to examine the effect of PCM thickness on temperature control, finding that a 5 cm thick PCM provided better cooling than a 3 cm thick one. However, increasing PCM thickness does not always improve temperature control. Bria et al. [42] studied six different PCM thicknesses, revealing that thinner PCMs melted quickly during the day, while thicker ones failed to fully melt, reducing thermal control efficiency. These findings suggest that there is an optimal thickness for PCM performance, a conclusion also supported by Zhou et al. [22].

In a PV-PCM system, both the properties of the PCMs and external environmental factors can significantly affect system efficiency [43]. Ahmed et al. [44] studied the economic potential of grid-connected PV power plants in five climatic regions of Pakistan, finding that environmental temperature, wind speed, and solar radiation strongly influence PV system performance. Jing et al. [45] confirmed similar results. Due to varying geographical locations and surrounding environments, there are regional differences in thermal and wind conditions [46], which in turn affect PV power generation. For instance, Meng et al. [47] analyzed 246 rooftop PV systems in different locations and found significant performance variations. Siala et al. [48] focused on the spatial analysis of PV power generation potential in the ASEAN region, noting that annual surface radiation ranged from 4.1 kWh/(m^2·d) to 5.1 kWh/(m^2·d), highlighting the relationship between geographical location and PV system performance. Qu et al. [49] investigated the optimal inclination of PV-PCM systems to enhance performance, while Farouk et al. [50] examined the impact of adding PV to roofs and walls, along with using PCM inside walls, on electricity production and energy consumption in Saudi Arabian residential buildings.

The above analysis shows that PCMs can effectively reduce the temperature of PV modules, improving their operational efficiency. However, in practical applications, the performance of PV module systems is influenced by factors such as phase-change temperature, thermal conductivity, material thickness, and environmental conditions. Previous research has mainly focused on the thermal properties of PCMs, but the diverse climatic and ecological conditions across China may significantly impact the performance of PV-PCM systems in different regions. To explore the characteristics and potential applications of PV-PCM systems in various climatic regions of China, this study uses numerical simulations to analyze thermal storage and release properties, as well as to determine the optimal configuration parameters for PV-PCM systems. The research employs a composite material of paraffin wax and expanded graphite as the phase-change material to assess nine regions in China.

2. Experiment Study

The experiment in this paper has been done in Jinan, Shangri-La, and Ganzi to compare the effects of PCM thermal management on PV. Two 1170 × 770 × 30 mm commercial monocrystalline silicon photovoltaic modules were used in the experiment. PCM thermal-management system was installed on the back of the PV module (PV-PCM) in Figure 1b, and the other PV model was set as the reference group (PV-ref) without the thermal-management method in Figure 1a. In the process of the experiment, two PV modules are mounted on the same base at the same Angle. The test sites were all open spaces or building roofs without shadow or shelter, and the experiment time was from 9:00 to 17:00 (Figure 2). The target monitoring parameters are PV temperature, PV power output, and local meteorological parameters. The parameters of the photovoltaic module are shown in Table 1, the information on measuring instruments can be found in Table 2.



Figure 1. Schematic drawing of two modules: (**a**) PV-ref and (**b**) PV-PCM.

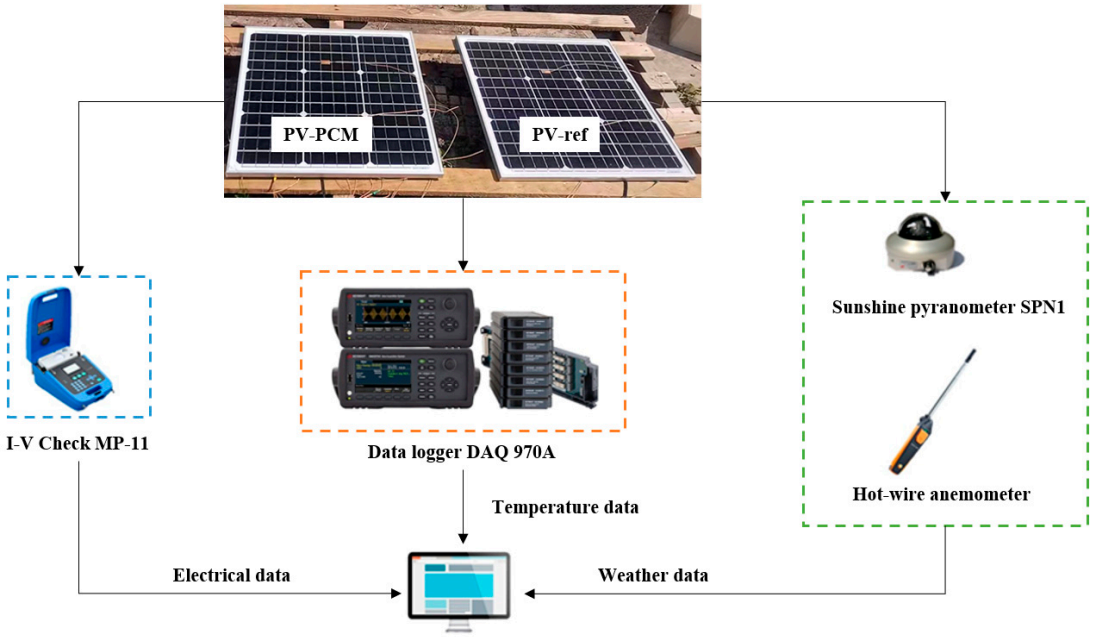


Figure 2. Real products of two modules.

Table 1. Parameters of the PV module used in this study.

Parameters	Unit	Values
Maximum power	W	170
Maximum power point voltage	V	20.83
Maximum power point current value	A	8.17
Open-circuit voltage	V	24.31
Short-circuit current	A	8.64
Dimension	mm	1170 × 770 × 30
Power tolerance	–	+/−3%

Table 2. Information of the instrument.

	Instrument	Product Number	Range	Accuracy
Temperature	data logger	DAQ970A (form Keysight Technologies, Santa Rosa, CA, USA)	−200 to 482 °C	±0.4%
Current Voltage	I–V characteristic curve instrument	EKO MP-11-SET-E (from EKO Instruments, Tokyo, Japan)	100 mA–30 A 10 V–1000 V	±1%
Environment temperature	temperature and humidity recorder	GSP-6 (from Greatech Scientific, Shanghai, China)	−40 to 80 °C	±0.5 °C
Wind velocity	hot-wire anemometer	Testo 405i (from Testo GmbH, Titisee-Neustadt, Germany)	0–30 m/s	±0.1 m/s
Solar irradiance	solar irradiance meter	Delta-T SPN1 (from Delta-T Devices, Cambridge, UK)	0–2000 W/m^2	5%

In this study, the paraffin PCM was modified with expanded graphite by means of mechanical mixing and vacuum impregnation. The ratio of 95% paraffin wax by mass fraction and 5% expanded graphite by mass fraction was selected. The preparation process of paraffin/expanded graphite composite phase-change material (PW-EG) is as follows: (1) 95% paraffin and 5% expanded graphite are divided into the multi-layer pavement and put into beakers; (2) Put the beaker into a vacuum drying oven at 90 °C and −0.1 MPa for 48 h of vacuum impregnation, take out the container every 6 h and stir well; (3) Take out the composite phase-change material and fill it into the acrylic container to obtain the paraffin/expanded graphite composite phase-change material. The preparation process of paraffin/expanded graphite composite phase-change material is shown in Figure 3. The modified paraffin/expanded graphite composite phase-change material solves the shortcomings of the low thermal conductivity of pure paraffin and, at the same time, has a certain setting effect and is easy to package. The properties of PCM after preparation are shown in Table 3. The PCM is heated and then imported into an acrylic packaging box, which is sized to fit the PV module (Figure 3) and then combined with the PV module. In order to prevent PCM leakage during packaging, we used a glue that is widely used in the engineering field and has been tested for reliability. After many tests, the packaging method can consider both efficiency and experimental requirements.

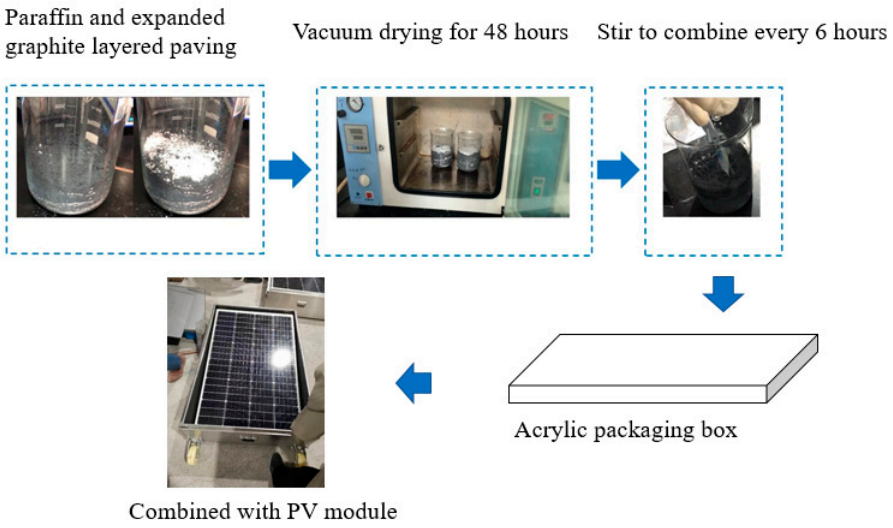


Figure 3. Preparation process of paraffin/expanded graphite composite phase-change materials.

Table 3. The properties of the PW/EG composite PCMs.

Property	Units	Value
Density	kg/m^3	950
Thermal conductivity	W/(m·K)	2.7
Specific heat	J/(kg·K)	1800, solid; 2000, liquid
Melting point	°C	41.5
Phase-change radius	°C	1.5
Latent heat	kJ/kg	177.7

The results of the experiment are presented in Figures 4–6. In particular, the performance of the PV-PCM system is significantly influenced by the temperature of the surrounding air in relation to the phase-change temperature of the PCM. In both Jinan and Shangri-La, the air temperature reaches or exceeds the melting point of the PCM (41.5 °C), therefore enabling the absorption of latent heat and the desired thermal-management effect. The PCM effectively absorbs heat before noon, therefore maintaining lower temperatures for the PV module and consequently enhancing the efficiency of the system. However, as the PCM melts and transitions into its liquid phase, the system's ability to dissipate heat

is reduced, resulting in a temporary rise in temperature after noon. In Ganzi, however, where the air temperature remains below the PCM's melting point, the PCM remains solid throughout the entire day, therefore acting as a thermal insulator rather than a thermal conductor. This results in a higher temperature for the PV-PCM module in comparison to the reference module (PV-ref) and does not enhance the power output. The inability of the PCM to reach its melting point precludes the realization of the anticipated benefits of thermal management, such as reduced temperature-induced degradation and increased power output. This demonstrates a limitation of PCMs in colder climates, where the ambient temperature is insufficient to initiate the phase-change process.

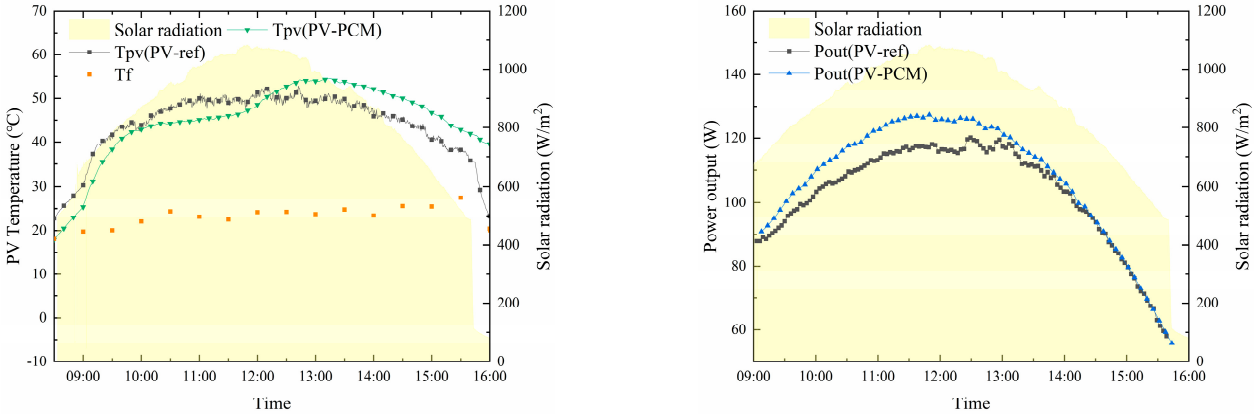


Figure 4. The PV temperature and power output in Jinan on 11 October 2022.

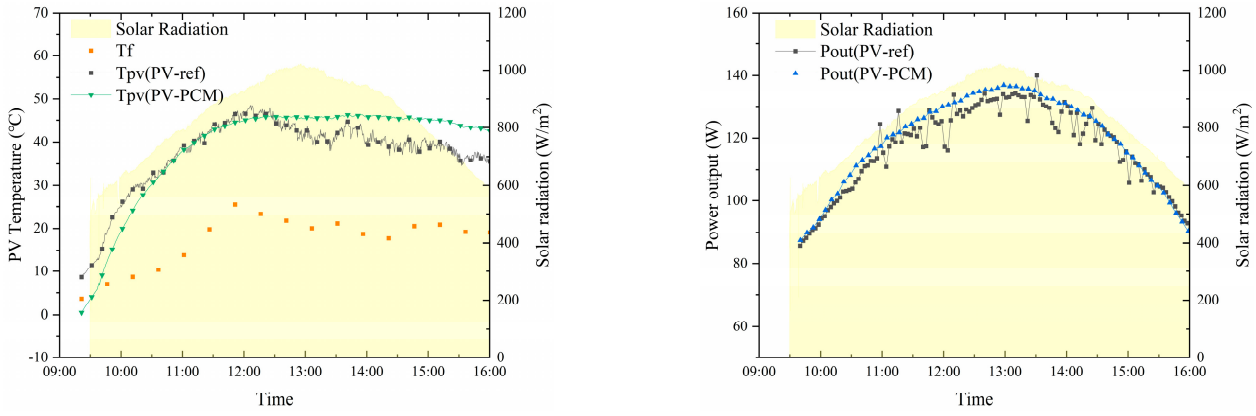


Figure 5. The PV temperature and power output in Shangri-La on 11 November 2022.

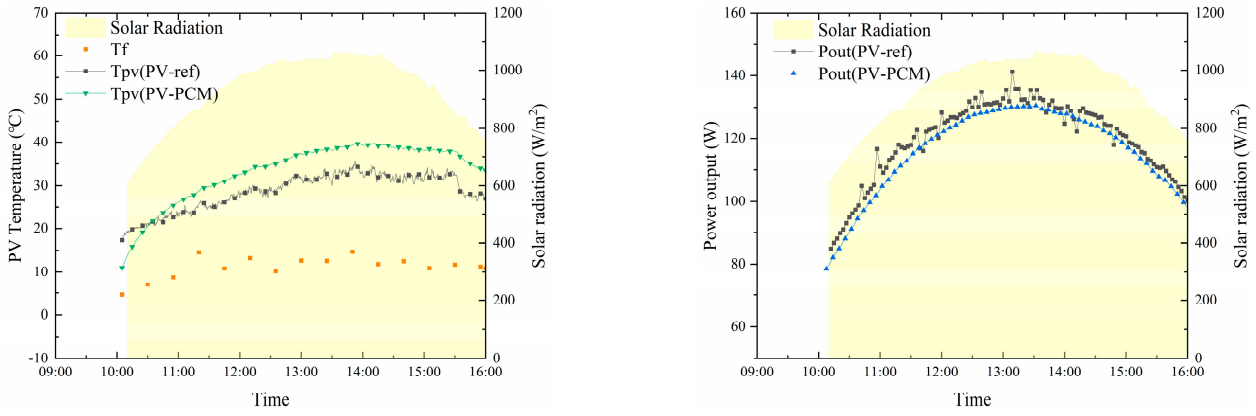


Figure 6. The PV temperature and power output in Ganzi on 17 November 2022.

In addition to environmental factors, the thermal properties of PCM itself also affect the power generation of PV-PCM. This is because when the PCM is solid, it increases thermal resistance, therefore preventing efficient heat dissipation from the PV module to the environment. This presents a duality: while it may prevent the PV module from overheating in certain conditions, it also prevents the system from benefiting from the latent heat absorption that the PCM provides in its melted state. In locations such as Ganzi, where the PCM remains in a solid state, this phenomenon results in a higher temperature for the PV module in comparison to a conventional PV system. Consequently, any potential advantages in power output are negated. Upon reaching its melting point, the PCM absorbs heat, therefore reducing the temperature of the PV module and preventing overheating, as demonstrated in Jinan and Shangri-La. Nevertheless, once the PCM has reached its melting point, it is no longer capable of providing active temperature control. Conversely, this results in an increase in thermal resistance due to alterations in the material properties, which in turn causes a rise in temperature in the afternoon. This transient behavior indicates that the efficacy of a PCM thermal-management system is contingent upon the timing and rate of phase change, which is subject to variation in accordance with climatic conditions.

3. Methods and Models

3.1. PV and PCM Heart Transfer Model

The heat transfer process is depicted in Figure 7. During the day, the front surface of the PV module absorbs solar radiation, which is partly converted into electrical output, reflected, and dissipated via convection and radiation. The rest of the energy is transformed into heat and transferred within the system. The heat is subsequently passed from the PV to the PCM, causing a reduction in surface temperature. At night, the heat stored in the PCM is released to the environment.

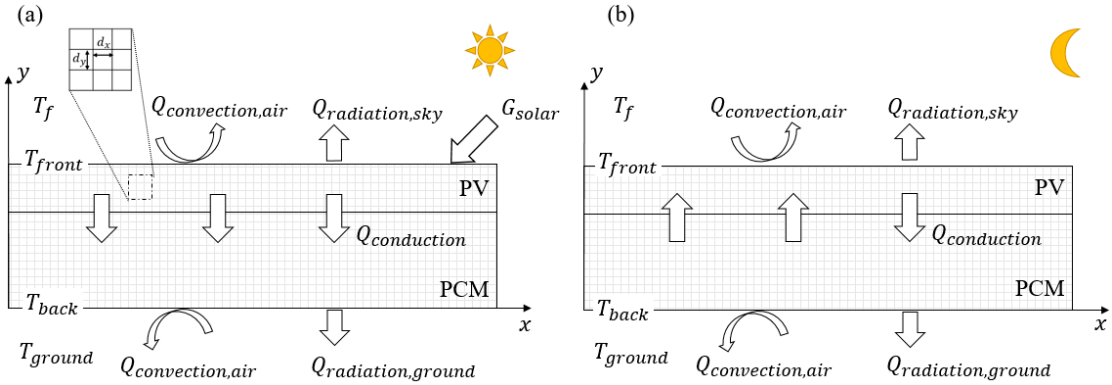


Figure 7. Heat transfer schematic diagram of the PV-PCM system. (**a**) heat transfer in the daytime (**b**) heat transfer at the nighttime.

When establishing the mathematical model of PV-PCM, the above heat transfer process is fully considered, and the following assumptions are made based on the actual situation:

(1) The natural convection inside the PCM is neglected. Only its conductive heat transfer is considered because the PCM is closely attached to the PV panel, and its internal state is stable [51].
(2) Other thermal properties of the PV module and phase-change material do not change with temperature, except for the specific heat capacity of the composite phase-change material [52].
(3) The thermal resistance between the surface of the PV module and the composite phase-change material in contact is ignored.

Based on the above assumptions, the two-dimensional control equations for the PV-PCM region are established as follows:

$$\rho c \frac{\partial T}{\partial \tau} = k \frac{\partial}{\partial x}\left(\frac{\partial T}{\partial x}\right) + k \frac{\partial}{\partial y}\left(\frac{\partial T}{\partial y}\right) + S \tag{1}$$

where ρ represents the density of each node, c represents the specific heat capacity of each node, k represents the thermal conductivity of each node, T represents the temperature of the node, and S represents the source term, which is defined as follows:

For the nodes inside the PV-PCM:

$$S = 0 \tag{2}$$

For the nodes in the front surface of the PV module:

$$S = \alpha G_{pv}(1-\eta) - \varepsilon_{glass}\sigma\left(T_{front}^4 - T_{sky}^4\right) - h_{front}\left(T_{front} - T_f\right) \tag{3}$$

For the nodes in the back surface of PCM:

$$S = -\varepsilon_{pcm}\sigma\left(T_{back}^4 - T_{ground}^4\right) - h_{back}\left(T_{back} - T_f\right) \tag{4}$$

where α is the absorptivity of the PV encapsulating glass, which is set as 0.9 in this study [53], G_{pv} is the total horizontal solar radiation reaching the PV front surface; η is the PV solar conversion efficiency; ε_{glass} and ε_{pcm} are the emissivities of the glass and PCM, respectively; σ represents the Stefan-Boltzmann constant; T_{front}, T_{back}, T_{sky}, T_{ground}, and T_f, are the temperatures of the front surface of the PV, the back surface of the PCM, the sky, the ground, and the air, respectively; h_{front} and h_{back} are the convective heat transfer coefficients of the front and back surfaces.

The sky equivalent temperature (T_{sky}) and ground temperature (T_{ground}) are calculated using the following equations [54]:

$$T_{sky} = 0.0375 T_f^{1.5} + 0.32 T_f \tag{5}$$

$$T_{ground} = T_f \tag{6}$$

The convective heat transfer coefficients for the front surface of the PV panel and the back surface of the PCM can be calculated using the following equations [55]:

$$h_{front} = 2.2v + 8.3 \tag{7}$$

$$h_{back} = 3.3v + 6.5 \tag{8}$$

where v is the wind velocity.

Furthermore, due to the changes in the properties of the PCM with temperature, this study adopted the heat capacity method to simulate this characteristic. Its definition is as follows:

$$c_{pcm} = \begin{cases} c_s, T < T_m - \delta T \\ ((c_s + c_l))/2 + LH/2\delta T, T_m - \delta T < T < T_m + \delta T \\ c_l, T > T_m + \delta T \end{cases} \tag{9}$$

where c_{pcm}, c_s, and c_l are the specific heat capacities of the PCM, solid PCM, and liquid PCM, respectively; T, T_m, and δT are the current temperature of the PCM, the phase-change temperature, and the phase-change radius of the PCM, respectively; and LH is the enthalpy of phase-change.

For any node in the PCM region, the liquid fraction (f_l) is defined using the following equation:

$$f_l = \begin{cases} 0, T < T_m - \delta T \\ (T - (T_m - \delta T)/2\delta T, T_m - \delta T < T < T_m + \delta T \\ 1, T > T_m + \delta T \end{cases} \tag{10}$$

Due to the increase in PV panel temperature, the power generation efficiency is reduced, so the actual power generation efficiency is calculated as follows [53].

$$\eta = \eta_{ref}\left[1 - \beta_{ref}\left(T_{pv} - T_{ref}\right)\right] \tag{11}$$

Therefore, the actual power generation of photovoltaic panels is calculated by the following equation [50].

$$P = \eta G_{pv} A_{pv} \tag{12}$$

where η, and β_{ref} are the actual photoelectric efficiency of the PV module, the reference photoelectric efficiency of the PV module, and the temperature coefficient of the PV module, respectively. T_{pv} and T_{ref} are the actual operating temperature of the PV module and the reference operating temperature under standard test conditions, respectively. P_{out} is the power output of the PV.

In this study, the PV model is discretized by the finite volume method and iterative solution method. To improve the computational efficiency, this study uses the combination of the tridiagonal matrix algorithm (TDMA) and alternating-direction implicit iteration (ADI) to accelerate the solving process, and all the solving processes are implemented in the FORTAN language.

3.2. Multi-Objective Optimization Method

Response Surface Methodology (RSM) is a statistical technique that leverages a systematic experimental design process to gather data from experiments. It employs a multivariate quadratic regression equation to establish a mathematical relationship between the factors and the response variable. Through the analysis of this regression equation, RSM aims to identify optimal process parameters and address multivariate challenges. Notably, RSM offers the advantage of investigating the synergistic impacts of multiple factors on the response variable while conducting a relatively limited number of experiments.

The analysis of RSM mainly involves the following processes:

(1) Determine the factors and levels: In this study, the main factors influencing the power generation of PV-PCM systems are determined through a literature review method. The factors identified are phase-change temperature (T_m), thermal conductivity of PCM (k_{pcm}), and thickness of PCM (δ_{pcm});
(2) Experimental design: In this study, the Box-Behnken design (BBD) method is adopted, which requires fewer experiments compared to the central composite design. It divides each influencing factor into three levels, namely the two endpoints and the midpoint;
(3) Conducting experiments and collecting data: In this study, the parameters of each experimental design point were inputted into a numerical simulation program for a year-long calculation;
(4) Fitting the response model and sensitivity analysis of the influencing factors;
(5) Response surface analysis.

In this study, T_m, k_{pcm}, and δ_{pcm} were chosen as the three parameters. Each parameter was divided into three levels represented by -1, 0, and 1. The main operating temperature of the PV panel is 25–65 °C [28,53], in order to ensure the temperature-control performance, the phase-change temperature of the selected phase-change material should be located in this interval. Since the melting point and latent heat of PCM are interrelated, the physical parameters are chosen according to the actual paraffin-based PCMs, which are 17 alkanes, 20 alkanes, and 24 alkanes, respectively. Increasing the thermal conductivity of paraffin wax by the addition of expanded graphite is recognized as a very suitable method, and its effect on the latent heat and thermal conductivity can be ignored due to its small addition amount. For the thickness of PCM, it cannot exceed the thickness of the PV panel border, which is 30 mm. The detailed factor levels and designed experimental scheme are shown in Tables 4 and 5, respectively.

Table 4. Influencing factors and levels.

Levels \ Factors	$X_1(T_m)$ °C	$X_2(k_{pcm})$ W/m·K	$X_3(\delta_{pcm})$ mm
−1	21.6	0.27	0
0	36.1	1.485	15
+1	50.6	2.7	30

Table 5. Box-Behnken design test scheme.

Standard Sequence Number	X_1	X_2	X_3
1	−1	−1	0
2	1	−1	0
3	−1	1	0
4	1	1	0
5	−1	0	−1
6	1	0	−1
7	−1	0	1
8	1	0	1
9	0	−1	−1
10	0	1	−1
11	0	−1	1
12	0	1	1
13	0	0	0
14	0	0	0
15	0	0	0
16	0	0	0
17	0	0	0

Within the PV-PCM system, it is essential to consider not only the potential increase in power generation resulting from the inclusion of PCM but also the associated cost increment. This cost increment primarily comprises the expenses related to PCM components, encompassing the cost of the PCM itself and the cost of packaging materials. This study uses a simple economic model, which is mainly cost increment analysis. Compared to PV without PCM, the incremental cost of PV-PCM comes from three components: phase-change materials (a mixture of paraffin and expanded graphite used in this study) and encapsulated enclosures (acrylic used in this study), their prices are shown in Table 6.

$$\text{Cost} = \text{W} \times \text{L} \times \delta \times \varphi \times d_{EG} \times P_{EG} + \text{W} \times \text{L} \times \delta \times (1-\varphi) \times d_P \times P_P + 2 \times (W+L) \times \delta \times \gamma \times d_A \times P_a \quad (13)$$

where W and L are the width and length of the component, respectively. δ is the thickness of the PCM, φ is the added proportion of expanded graphite, d_{EG}, d_P and d_A are the density of expanded graphite, paraffin, and acrylic, respectively. P_{EG}, P_P and P_a are the prices of expanded graphite, paraffin, and acrylic, respectively. γ is the width of the acrylic.

Table 6. The prices of materials used in this study.

	Paraffin (CNY/ton)	Expanded Graphite (CNY/ton)	Acrylic (CNY/m^3)
Prices	6500	3600	20.0

In this study, increasing power generation and decreasing additional costs are two objectives, and T_m, k_{pcm}, and δ_{pcm} are taken as optimization variables. The multi-objective optimization model and constraints are shown below:

$$minY = [y_1(x), -y_2(x)] \quad (14)$$

$$s.t. \begin{cases} g_i(x) \le 0, i = 1,2 \\ h_i(x) = 0, i = 1,2 \end{cases} \quad (15)$$

$$X = (x_1, x_2, x_3) \quad (16)$$

where Y is the set of objective functions; y_1 is the cost increment objective function, $-y_2$ is the generation increment objective function, X is the decision space; $g_i(x)$ is an inequality constraint; $h_i(x)$ is an equality constraint.

4. Results and Discussion

4.1. Location Selection

As previously mentioned, meteorological factors (e.g., radiation, temperature, etc.) play a significant role in influencing the power generation efficiency of PV-PCM systems. To comprehensively assess the utilization potential of PV-PCM systems across various regions of China, this study initially aimed to encompass all five climate regions utilized in building thermal design within China. This approach allowed for a thorough examination of the impact of temperature. Ultimately, the study selected two cities from each climate region, each with distinct levels of solar radiation, as specific subjects for investigation. Notably, in the temperate region, solar radiation levels remain relatively consistent, resulting in only one city being studied in this particular zone. Table 7 lists all study cities.

Table 7. The cities in this study.

Climate Region	Grade of Solar Energy Resources	Cities	Annual Total Horizontal Radiation (kWh/m^2)
1B	A	Naqu	1869
1C	B	Ganzi	1701
2A	B	Lanzhou	1596
2B	A	Lhasa	1941
3A	C	Chengdu	1083
3B	B	Nanjing	1398
4A	C	Hechi	1235
4B	B	Sanya	1557
5A	B	Chuxiong	1623

It can be seen from Figure 8a,b that the nine selected cities have significant differences in annual daily hourly solar radiation and temperature. Take Naqu as an example. Its solar radiation level is high, while its temperature is the lowest among the selected regions. On the contrary, Chengdu has a low solar radiation level among the selected objects, but its temperature is at a medium level. Therefore, it can be considered that the selected city can better consider the influence of solar radiation and temperature in different regions of China on PV-PCM components.

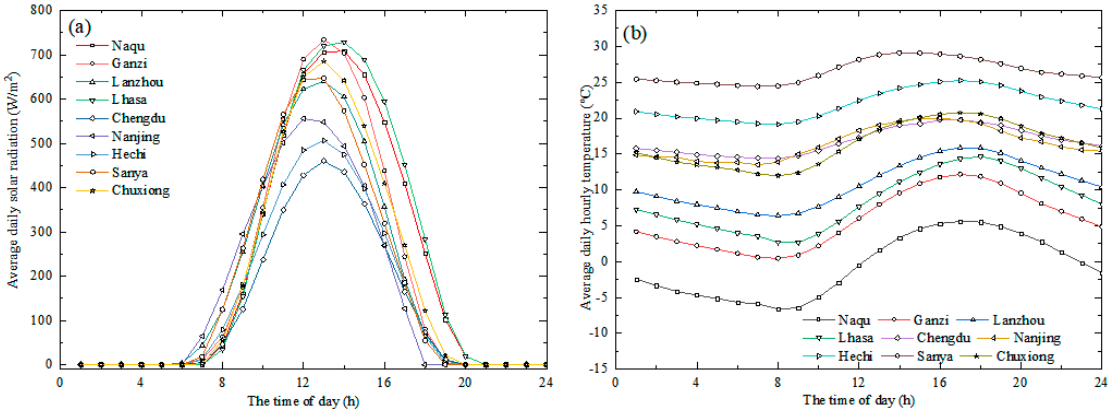


Figure 8. Annual daily hourly solar radiation and temperature of the nine selected cities: (**a**) solar radiation, (**b**) temperature.

4.2. Response Surface Model

Numerical simulations with different levels of influencing factors are carried out in Table 4. Response models that represent the response relationship between each influencing factor and the target can be obtained based on second-order polynomial equations, and each response model contains a constant term, a linear term, an interaction term, and a squared term. Based on the simulation results, the response functions for the full-year power generation enhancement of the PV-PCM system in different regions can be obtained, as shown in Table 8. The larger the F-value and the smaller the p-value, the more significant the model or term is. In general, a p-value of less than 0.05 is considered significant, and the correlation is strong, while a p-value greater than 0.1 indicates that the item is not significant and can be considered to be removed appropriately. As shown in Table 7, the values of R^2 collectively show that the model is statistically significant and highly accurate.

Table 8. Summary of response surface model.

City	Response Surface Model	
Naqu	$RF_1 = 2.63451 - 0.18328X_1 + 1.19996X_2 + 0.06278X_3 + 0.00736X_1X_2 - 0.00310X_1X_3 + 0.04407X_2X_3 + 0.00225X_1^2 - 0.46528X_2^2 - 0.000239X_3^2$	$R^2 = 0.8680$ $p = 0.0214$
Ganzi	$RF_2 = 1.08771 - 0.13314X_1 + 2.58362X_2 + 0.24736X_3 + 0.009263X_1X_2 - 0.006829X_1X_3 + 0.065455X_2X_3 + 0.001465X_1^2 - 0.9096X_2^2 - 0.0011196X_3^2$	$R^2 = 0.9172$ $p = 0.0048$
Lanzhou	$RF_3 = -10.3392 + 0.5270X_1 + 3.3670X_2 + 0.05489X_3 + 0.0045523X_1X_2 - 0.004977X_1X_3 + 0.072248X_2X_3 - 0.00749102X_1^2 - 1.14855X_2^2 + 0.00176128X_3^2$	$R^2 = 0.9957$ $p < 0.0001$
Lhasa	$RF_4 = 0.40489 - 0.11555X_1 + 3.11928X_2 + 0.20016X_3 + 0.012542X_1X_2 - 0.007434X_1X_3 + 0.079263X_2X_3 + 0.001251X_1^2 - 1.12106X_2^2 - 0.0001451X_3^2$	$R^2 = 0.9099$ $p = 0.0064$
Chengdu	$RF_5 = -8.2045 + 0.4347X_1 + 2.00263X_2 + 0.10723X_3 + 0.002242X_1X_2 - 0.001734X_1X_3 + 0.03963X_2X_3 - 0.00611X_1^2 - 0.67371X_2^2 - 0.001832X_3^2$	$R^2 = 0.9903$ $p < 0.0001$
Nanjing	$RF_6 = -7.92811 + 0.40262X_1 + 2.35298X_2 + 0.038698X_3 + 0.00368668X_1X_2 - 0.00219977X_1X_3 + 0.055881X_2X_3 - 0.00566403X_1^2 - 0.78873X_2^2 - 0.000520X_3^2$	$R^2 = 0.9924$ $p < 0.0001$
Hechi	$RF_7 = -12.54404 + 0.62001X_1 + 3.80347X_2 + 0.22247X_3 + 0.00181X_1X_2 - 0.001335X_1X_3 + 0.01686X_2X_3 - 0.00861X_1^2 - 1.17591X_2^2 - 0.00463X_3^2$	$R^2 = 0.9654$ $p = 0.0003$
Sanya	$RF_8 = -25.58307 + 1.39182X_1 + 4.51378X_2 + 0.024051X_3 - 0.002725X_1X_2 - 0.000768X_1X_3 + 0.092424X_2X_3 - 0.019174X_1^2 - 1.4319X_2^2 - 0.002187X_3^2$	$R^2 = 0.9488$ $p = 0.0010$
Chuxiong	$RF_9 = -4.28822 + 0.16741X_1 + 3.22283X_2 + 0.21662X_3 + 0.007091X_1X_2 - 0.006018X_1X_3 + 0.07245X_2X_3 - 0.002661X_1^2 - 1.07838X_2^2 - 0.001552X_3^2$	$R^2 = 0.9565$ $p = 0.0006$

The response surface model shows that X_2 and X_2^2 have more significant effects on the response model overall, indicating that the thermal conductivity of PCM has a greater effect on the energy storage rate and the amount. On the other hand, the significant terms of the response model are different in different regions. For example, in Nanjing, the significant terms are X_1, X_2, and X_2^2, the melting point and thermal conductivity have greater impacts on power generation, and the interaction term is not significant on the annual power generation enhancement. In Ganzi, Sichuan, the significant terms are X_2, X_3, and X_2^2, which means that the thermal conductivity and the amount of PCM have a more significant effect on the annual power generation. Observations reveal that in regions like Ganzi and Nagqu, characterized by lower temperatures and ample solar energy resources, there exists a wider temperature differential between the environment and the PV module. As a result, the phase-change temperature exerts a comparatively minor influence on the PCM melting process. Conversely, in regions with higher air temperatures, such as Nanjing and Sanya, the choice of the phase-change temperature assumes significant importance and directly impacts the melting process. In these locales, a comprehensive consideration of the interplay between various physical parameters is essential to avoid the premature occurrence of complete melting.

4.3. Optimization Results and Discussion

According to the response model of each climate zone, a multi-objective optimization program based on the NSGA-II algorithm was written in Matlab 2020a software to obtain the Pareto frontiers of the optimal design parameters of the PV-PCM system in each region under conflicting objectives, and Pareto frontiers of the optimal design parameters can be obtained in each region.

As shown in Supplementary Materials it is worth noting that the Naqu region exhibits different outcomes, in which the use of PCM may also lead to a decline in power generation. The ideal phase-change temperature is at the lower limit temperature, and in order to enhance the power generation of the PV module, the thermal conductivity and volume must reach a sufficient level. The temperature in the Nagqu region is typically low, and there is strong solar radiation throughout the year. As a result, the PCM cannot melt in winter to play the temperature control around, and in summer, it is easy to melt too early to hinder the heat dissipation of the PV module, so it is necessary to increase the thermal conductivity and the amount of to ensure that the temperature-control system has a great heat storage rate and heat storage, but this will result in a significant increase in cost. Therefore, it can be assumed that phase-change temperature control is not suitable for cold regions.

The set of optimal solutions in the Ganzi region is shown in Supplementary Materials. Most of the optimal phase-change temperature is concentrated around 21.6 °C, which is close to the lower limit, and the thickness of the phase transition material is more uniformly distributed in the feasible domain. With the increase of the thickness of the phase transition material, the temperature-control effect is enhanced, and the power generation capacity is also gradually increased. As for the Nanjing area, the optimal phase-change temperature is distributed at 30–34 °C. To ensure the melting rate, the increase in the amount of PCM corresponds to higher thermal conductivity, but at the same time, the optimal phase-change temperature will also be reduced, which can enlarge the operation range of PCM.

The data are for the working conditions with the largest power generation in the Pareto frontier distribution, which corresponds to the largest cost increment (Table 9). It can be seen that the annual power generation of PV modules in each region is sorted from largest to smallest in the same order as the total annual solar irradiation. Except for Naqu, PCM can improve the annual power generation, with improvement ratios ranging from 1.4% to 3%.

Table 9. Optimal parameters of PCM in different cities.

	X_1 (°C)	X_2 (W/m K)	X_3
Naqu	21.6	2.7	30
Ganzi	21.6	2.61	30
Lanzhou	25.93	2.46	30
Lhasa	21.6	2.57	30
Chengdu	31.78	2.42	30
Nanjing	30.51	2.63	30
Hechi	34.54	1.8	22.35
Sanya	35.52	2.51	30
Chuxiong	21.6	2.57	30

Combined with the time-by-time variations of panel temperature and melting fraction in Figures 9 and 10, it can be found that the temperatures are lower in winter, so the PV panels dissipate heat better, and thus, their temperatures are lower, resulting in a very low overall melting fraction of PCM, around 0.1. Compared with Sanya, Chuxiong, Hechi, and other areas with higher temperatures, Chuxiong has the strongest solar radiation, and thus, PCM gives full play to its temperature-control role. In summer, the melting fraction of PCMs is generally higher, but for the Chuxiong and Hechi areas, it is easy to appear the condition that the PCM cannot be completely melted at night, which affects

the temperature-control performance on the next day. However, from the perspective of the whole year, the improvement in annual power generation is more pronounced in areas with high average annual temperatures and very rich solar resources or high summer temperatures and rich solar resources. As shown in the Supplementary Materials, compared to cost increment and power generation increment, the phase-change thermal-management system is not economical.

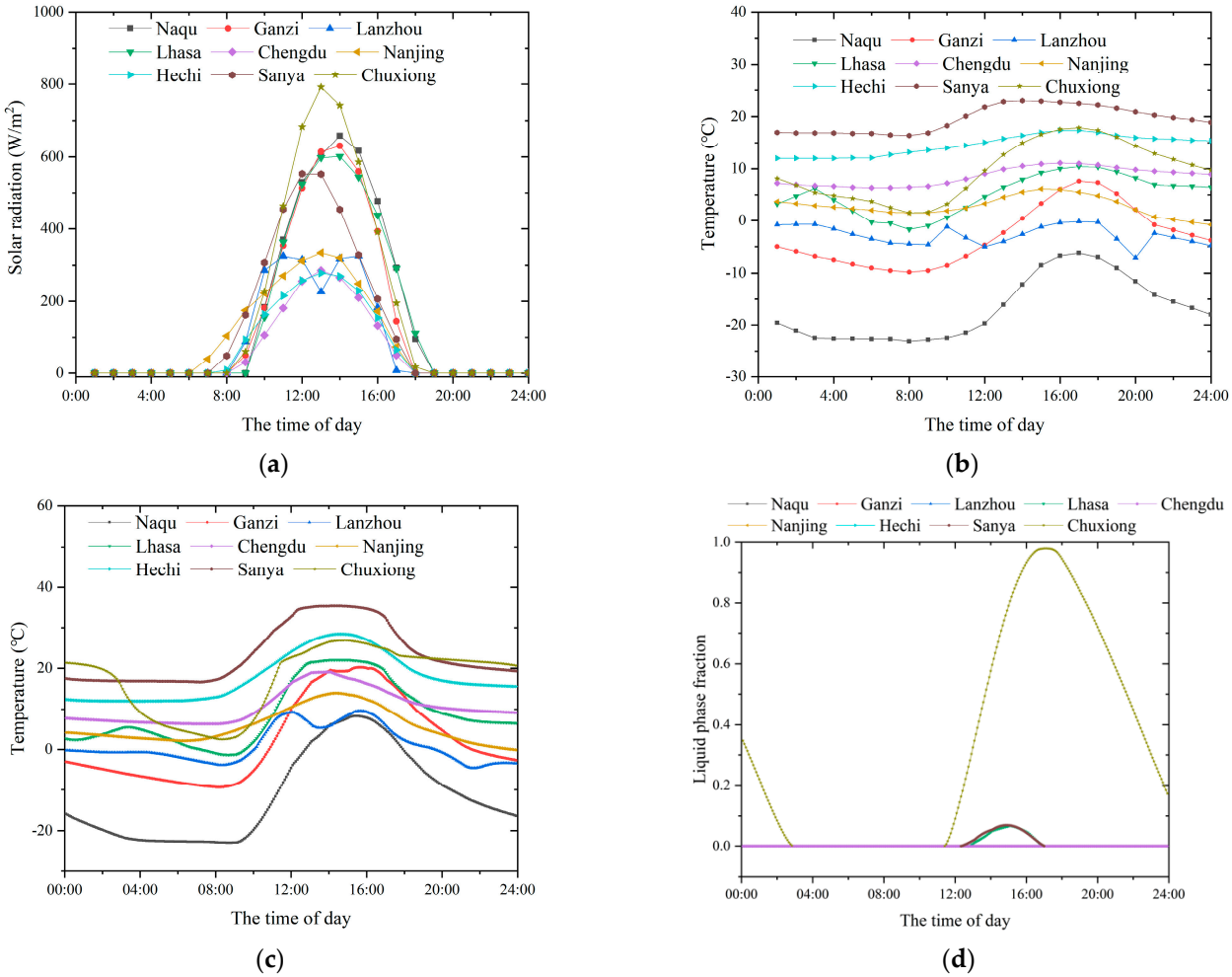


Figure 9. Thermal-management performance on a typical day of winter. (**a**) Solar radiation (**b**) Air temperature. (**c**) Temperature of PV panel (**d**) Liquid fraction of PCM.

Figure 11 shows the effect of the power generation improvement of PV modules in the above regions after the introduction of PCM. Among all the regions, the power generation improvement in Nagqu is very poor, only about 0.5%, because Nagqu is a cold region with an average annual temperature below 20 °C. Similar to Ganzi, Lhasa is a region with low temperature but good solar radiation, and the power generation improvement effect is between 2% and 3%. Chuxiong and Hechi, as well as Sanya and other regions, have generally high temperatures throughout the year, and PCM can also be effective. The Chengdu region has poor solar radiation, but due to high summer temperatures, PCM can also reduce the temperature of PV panels. Overall, phase-change control technology can achieve a 1.4–3% increase in PV module power generation, except for Naqu.

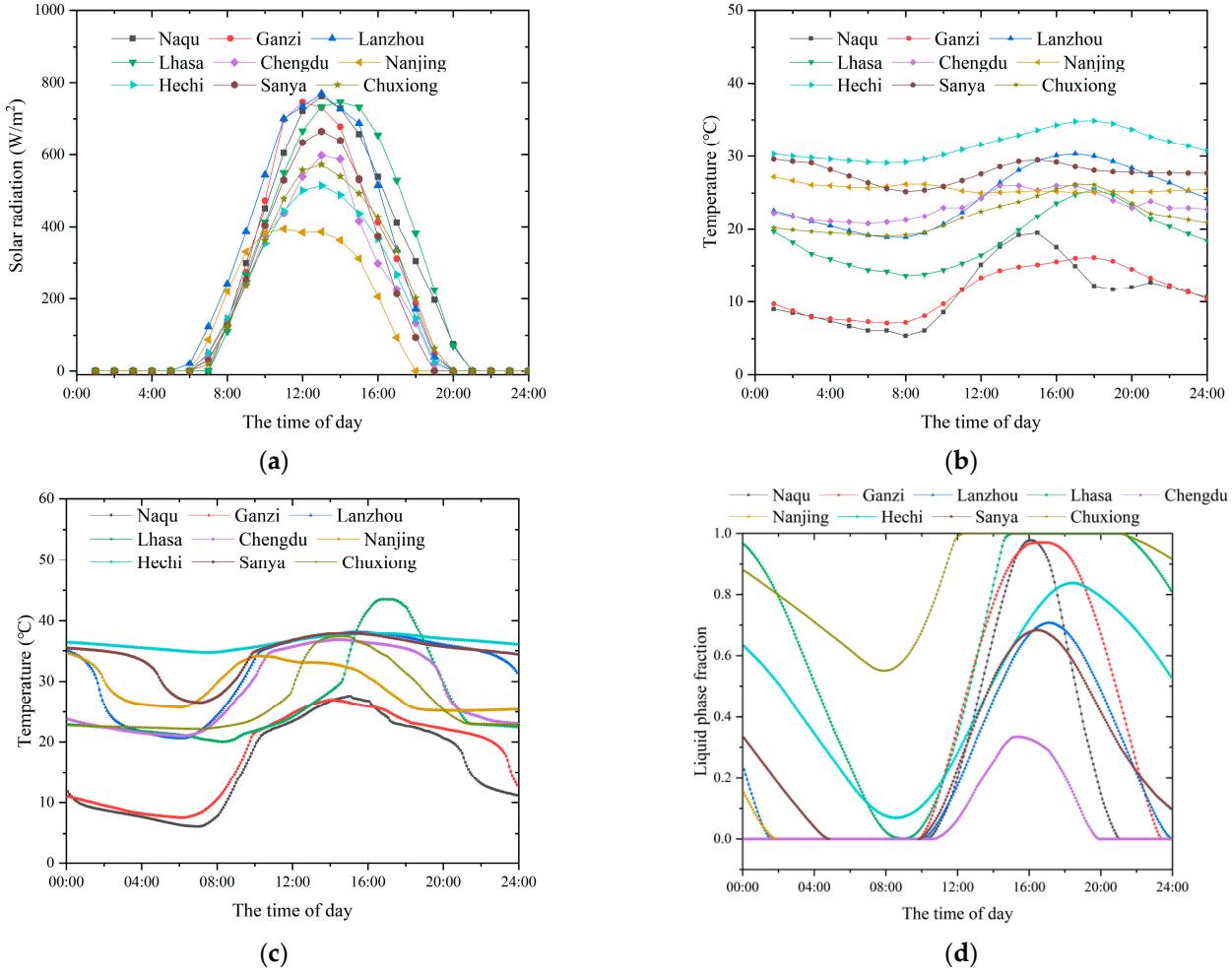


Figure 10. Thermal-management performance on a typical day of Summer. (**a**) Solar radiation (**b**) Air temperature. (**c**) Temperature of PV panel (**d**) Liquid fraction of PCM.

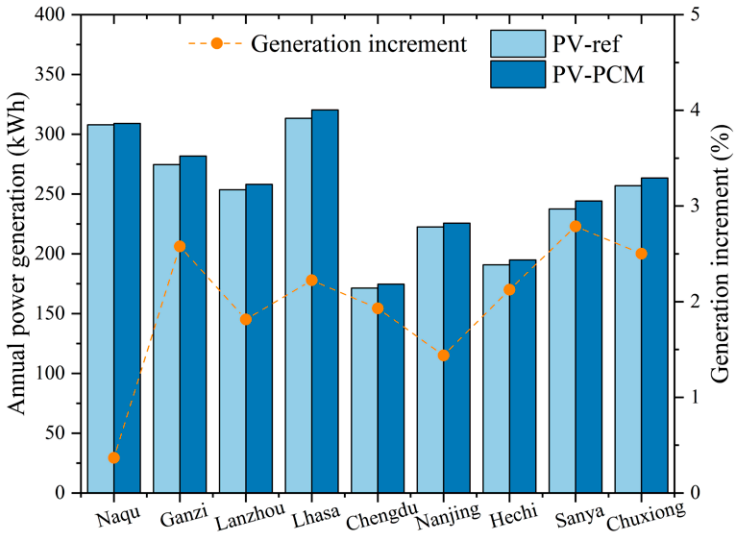


Figure 11. Power generation in different regions.

5. Conclusions

The research assesses the temperature regulation capabilities of PV modules experimentally and numerically. For the annual assessment of PV-PCM system operation, nine distinct regions in China have been investigated through numerical simulations. A multi-objective optimization design is undertaken using the Response Surface-NSGA-II method, focusing on two key objectives: augmenting annual power generation and managing system cost increases. The decision variables in this optimization process include the melting point, thermal conductivity, and thickness of the PCM. The results show that:

(1) It is revealed that the temperature-control performance of PCM is affected by the intensity of solar radiation and climatic conditions through experiments, so the design parameters of PCM should be decided according to the local conditions.
(2) Based on the two mutually exclusive objectives of annual power generation enhancement and cost increase of the system, a series of Pareto solutions for the design parameters of the phase-change thermal-management system in nine regions of China are obtained, which can provide a reference for the optimal design of temperature control with PCM.
(3) In extremely cold regions such as Naqu, PCM is basically ineffective in regulating temperature and its annual power generation is only increased by 0.5%. Conversely, for the other regions investigated in this paper, the utilization of PCM can enhance annual power generation, with improvements ranging from 1.4% to 3%. In summary, the increase in annual power generation is more substantial in regions characterized by high average annual temperatures and abundant solar resources, as well as in areas with high summer temperatures and ample solar resources.
(4) Considering the combination of life-cycle gains and initial investment, PCM temperature-control technology for PV modules is economically inefficient and unsuitable for application in practical projects.

In future work, considering the significant impact of climate conditions on PCM performance, it is recommended to tailor the selection of PCM type and thickness based on the specific climatic characteristics of different regions. In areas with high solar radiation and warm climates, PCM can provide a noticeable increase in energy yield, making it suitable for application in such regions. Conversely, in colder climates, alternative thermal-management solutions or adjustments to the PCM material may be necessary to optimize overall PV system performance. By accurately selecting and configuring PCM according to local climate data and market demands, the economic viability and sustainability of PV systems can be effectively enhanced.

Supplementary Materials: The following supporting information can be downloaded at: https://www.mdpi.com/article/10.3390/en17236200/s1, Table S1 Optimal solution set in Naqu. Table S2 Optimal solution set in Ganzi. Table S3 Optimal solution set in Lanzhou. Table S4 Optimal solution set in Lhasa. Table S5 Optimal solution set in Chengdu. Table S6 Optimal solution set in Nanjing. Table S7 Optimal solution set in Hechi. Table S8 Optimal solution set in Sanya. Table S9 Optimal solution set in Chuxiong.

Author Contributions: Conceptualization, X.C.; Methodology, L.T., Y.L. and L.Y.; Software, J.L.; Validation, L.Y.; Formal analysis, X.C.; Writing—original draft, L.T.; Writing—review & editing, X.C.; Supervision, Y.L.; Funding acquisition, L.T. All authors have read and agreed to the published version of the manuscript.

Funding: This research is supported by the key technology of temperature control and efficiency improvement of double-sided double-glass photovoltaic modules and the implementation path of industrialization (37-K2023-128).

Data Availability Statement: The original contributions presented in the study are included in the article/Supplementary Materials, further inquiries can be directed to the corresponding author.

Conflicts of Interest: Authors Liang Tang, Yong Luo, Linlin Yin were employed by the company Shandong Electric Power Engineering Consulting Corp., Ltd. The remaining authors declare that

the research was conducted in the absence of any commercial or financial relationships that could be construed as a potential conflict of interest.

References

1. Thompson, H. The geopolitics of fossil fuels and renewables reshape the world. *Nature* **2020**, *603*, 354. [CrossRef] [PubMed]
2. IRENA. *World Energy Transitions Outlook: 1.5 °C Pathway*; International Renewable Energy Agency: Abu Dhabi, United Arab Emirates, 2021.
3. IRENA. *Renewable Energy Statistics 2020*; The International Renewable Energy Agency: Abu Dhabi, United Arab Emirates, 2020.
4. IRENA. *Renewable Capacity Statistics 2020*; The International Renewable Energy Agency: Abu Dhabi, United Arab Emirates, 2021.
5. Green, M.A. Photovoltaic principles. *Phys. E Low-Dimens. Syst. Nanostructures* **2002**, *14*, 11–17. [CrossRef]
6. Skoplaki, E.; Palyvos, J.A. On the temperature dependence of photovoltaic module electrical performance: A review of efficiency/power correlations. *Sol. Energy* **2009**, *83*, 614–624. [CrossRef]
7. Ma, T.; Yang, H.; Zhang, Y.; Lu, L.; Wang, X. Using phase change materials in photovoltaic systems for thermal regulation and electrical efficiency improvement: A review and outlook. *Renew. Sustain. Energy Rev.* **2015**, *43*, 1273–1384. [CrossRef]
8. Teo, H.G.; Lee, P.S.; Hawlader, M.N.A. An active cooling system for photovoltaic modules. *Appl. Energy* **2012**, *90*, 309–315. [CrossRef]
9. Sajjad, U.; Amer, M.; Ali, H.M.; Dahiya, A.; Abbas, N. Cost effective cooling of photovoltaic modules to improve efficiency. *Case Stud. Therm. Eng.* **2019**, *14*, 100420. [CrossRef]
10. Jun Huang, M. The effect of using two PCMs on the thermal regulation performance of BIPV systems. *Sol. Energy Mater. Sol. Cells* **2011**, *95*, 957–963. [CrossRef]
11. Nižetić, S.; Papadopoulos, A.M.; Giama, E. Comprehensive analysis and general economic-environmental evaluation of cooling techniques for photovoltaic panels. Part I: Passive cooling techniques. *Energy Convers. Manag.* **2017**, *149*, 334–354. [CrossRef]
12. Soares, N.; Costa, J.J.; Gaspar, A.R.; Santos, P. Review of passive PCM latent heat thermal energy storage systems towards buildings' energy efficiency. *Energy Build.* **2013**, *59*, 82–103. [CrossRef]
13. Tan, L.; Date, A.; Fernandes, G.; Singh, B.; Ganguly, S. Efficiency Gains of Photovoltaic System Using Latent Heat Thermal Energy Storage. *Energy Procedia* **2017**, *110*, 83–88. [CrossRef]
14. Stropnik, R.; Stritih, U. Increasing the efficiency of PV panel with the use of PCM. *Renew. Energy* **2016**, *97*, 671–679. [CrossRef]
15. Hasan, A.; Sarwar, J.; Alnoman, H.; Abdelbaqi, S. Yearly energy performance of a photovoltaic-phase change material (PV-PCM) system in hot climate. *Sol. Energy* **2017**, *146*, 417–429. [CrossRef]
16. Díaz, F.A.; Moraga, N.O.; Cabrales, R.C. Computational modeling of a PV-PCM passive cooling system during a day–night cycle at arid and semi-arid climate zones. *Energy Convers. Manag.* **2022**, *270*, 116202. [CrossRef]
17. Chen, J.; Kang, S.E.J.; Huang, Z.; Wei, K.; Zhang, B.; Liao, G. Effects of different phase change material thermal management strategies on the cooling performance of the power lithium ion batteries: A review. *J. Power Sources* **2019**, *442*, 227228. [CrossRef]
18. Sargunanathan, S.; Elango, A.; Mohideen, S.T. Performance enhancement of solar photovoltaic cells using effective cooling methods: A review. *Renew. Sustain. Energy Rev.* **2016**, *64*, 382–393. [CrossRef]
19. Machniewicz, A.; Knera, D.; Heim, D. Effect of transition temperature on efficiency of PV/PCM panels. *Energy Procedia* **2015**, *78*, 1684–1689. [CrossRef]
20. Browne, M.C.; Norton, B.; McCormack, S.J. Phase change materials for photovoltaic thermal management. *Renew. Sustain. Energy Rev.* **2015**, *47*, 762–782. [CrossRef]
21. Hasan, A.; McCormack, S.J.; Huang, M.J.; Sarwar, J.; Norton, B. Increased photovoltaic performance through temperature regulation by phase change materials: Materials comparison in different climates. *Sol. Energy* **2015**, *115*, 264–276. [CrossRef]
22. Zhou, X.; Cao, X.; Leng, Z.; Zhou, X.; Liu, S. Study on the temperature control performance of photovoltaic module by a novel phase change material/heat pipe coupled thermal management system. *J. Energy Storage* **2023**, *64*, 107200. [CrossRef]
23. Watanabe, T.; Kikuchi, H.; Kanzawa, A. Enhancement of charging and discharging rates in a latent heat storage system by use of PCM with different melting temperatures. *Heat Recover Syst. CHP* **1993**, *13*, 57–66. [CrossRef]
24. Qureshi, Z.A.; Ali, H.M.; Khushnood, S. Recent advances on thermal conductivity enhancement of phase change materials for energy storage system: A review. *Int. J. Heat Mass. Transf.* **2018**, *127*, 838–856. [CrossRef]
25. Khanna, S.; Reddy, K.S.; Mallick, T.K. Optimization of finned solar photovoltaic phase change material (finned pv pcm) system. *Int. J. Therm. Sci.* **2018**, *130*, 313–322. [CrossRef]
26. Gad, R.; Mahmoud, H.; Ookawara, S.; Hassan, H. Evaluation of thermal management of photovoltaic solar cell via hybrid cooling system of phase change material inclusion hybrid nanoparticles coupled with flat heat pipe. *J. Energy Storage* **2023**, *57*, 106185. [CrossRef]
27. Das, D.; Bordoloi, U.; Kamble, A.D.; Muigai, H.H.; Pai, R.K.; Kalita, P. Performance investigation of a rectangular spiral flow PV/T collector with a novel form-stable composite material. *Appl. Therm. Eng.* **2021**, *182*, 116035. [CrossRef]
28. Karthikeyan, V.; Sirisamphanwong, C.; Sukchai, S.; Sahoo, S.K.; Wongwuttanasatian, T. Reducing PV module temperature with radiation based PV module incorporating composite phase change material. *J. Energy Storage* **2020**, *29*, 101346. [CrossRef]
29. Asefi, G.; Ma, T.; Wang, R. Parametric investigation of photovoltaic-thermal systems integrated with porous phase change material. *Appl. Therm. Eng.* **2022**, *201*, 117727. [CrossRef]

30. Xiao, X.; Zhang, P.; Li, M. Preparation and thermal characterization of paraffin/metal foam composite phase change material. *Appl. Energy* **2013**, *112*, 1357–1366. [CrossRef]
31. Cheng, W.L.; Li, W.W.; Nian, Y.L.; Xia, W.D. Study of thermal conductive enhancement mechanism and selection criteria of carbon-additive for composite phase change materials. *Int. J. Heat Mass. Transf.* **2018**, *116*, 507–511. [CrossRef]
32. Karaipekli, A.; Biçer, A.; Sarı, A.; Tyagi, V.V. Thermal characteristics of expanded perlite/paraffin composite phase change material with enhanced thermal conductivity using carbon nanotubes. *Energy Convers. Manag.* **2017**, *134*, 373–381. [CrossRef]
33. Wang, C.; Lin, T.; Li, N.; Zheng, H. Heat transfer enhancement of phase change composite material: Copper foam/paraffin. *Renew. Energy* **2016**, *96*, 960–965. [CrossRef]
34. Ling, Z.; Chen, J.; Xu, T.; Fang, X.; Gao, X.; Zhang, Z. Thermal conductivity of an organic phase change material/expanded graphite composite across the phase change temperature range and a novel thermal conductivity model. *Energy Convers. Manag.* **2015**, *102*, 202–208. [CrossRef]
35. Harish, S.; Orejon, D.; Takata, Y.; Kohno, M. Thermal conductivity enhancement of lauric acid phase change nanocomposite with graphene nanoplatelets. *Appl. Therm. Eng.* **2015**, *80*, 205–211. [CrossRef]
36. Sari, A.; Karaipekli, A. Thermal conductivity and latent heat thermal energy storage characteristics of paraffin/expanded graphite composite as phase change material. *Appl. Therm. Eng.* **2007**, *27*, 1271–1277. [CrossRef]
37. Afaynou, I.; Faraji, H.; Choukairy, K.; Arıcı, M.; Khallaki, K. Heat transfer improvement of phase change materials by metal foams and nanoparticles for efficient electronic thermal management: A comprehensive study. *Int. J. Heat Mass. Transf.* **2024**, *227*, 125534. [CrossRef]
38. Faraji, H.; Teggar, M.; Arshad, A.; Arıcı, M.; Berra, E.M.; Choukairy, K. Lattice Boltzmann simulation of natural convection heat transfer phenomenon for thermal management of multiple electronic components. *Therm. Sci. Eng. Prog.* **2023**, *45*, 102126. [CrossRef]
39. Zhang, Y.; Ding, J.; Wang, X.; Yang, R.; Lin, K. Influence of additives on thermal conductivity of shape-stabilized phase change material. *Sol. Energy Mater. Sol. Cells* **2006**, *90*, 1692–1702. [CrossRef]
40. Naseer, A.; Jamil, F.; Ali, H.M.; Ejaz, A.; Khushnood, S.; Ambreen, T.; Khan, M.S.; Bashir, M.A.; Pao, W.; Yan, W.M. Role of phase change materials thickness for photovoltaic thermal management. *Sustain. Energy Technol. Asses.* **2022**, *49*, 101719. [CrossRef]
41. Ho, C.J.; Chou, W.L.; Lai, C.M. Thermal and electrical performance of a water-surface floating PV integrated with a water-saturated MEPCM layer. *Energy Convers. Manag.* **2015**, *89*, 862–872. [CrossRef]
42. Bria, A.; Raillani, B.; Chaatouf, D.; Salhi, M.; Amraqui, S.; Mezrhab, A. Effect of PCM thickness on the performance of the finned PV/PCM system. *Mater. Today Proc.* **2023**, *72*, 3617–3625. [CrossRef]
43. Maghami, M.R.; Hizam, H.; Gomes, C.; Radzi, M.A.; Rezadad, M.I.; Hajighorbani, S. Power loss due to soiling on solar panel: A review. *Renew. Sustain. Energy Rev.* **2016**, *59*, 1307–1316. [CrossRef]
44. Ahmed, N.; Naveed Khan, A.; Ahmed, N.; Aslam, A.; Imran, K.; Sajid, M.B.; Waqas, A. Techno-economic potential assessment of mega scale grid-connected PV power plant in five climate zones of Pakistan. *Energy Convers. Manag.* **2021**, *237*, 114097. [CrossRef]
45. Jing, J.; Zhou, Y.; Wang, L.; Liu, Y.; Wang, D. The spatial distribution of China's solar energy resources and the optimum tilt angle and power generation potential of PV systems. *Energy Convers. Manag.* **2023**, *283*, 116912. [CrossRef]
46. Chang, H.; Xiang, C.; Duan, C.; Wan, Z.; Liu, Y.; Zheng, Y.; Shang, Y.; Liu, M.; Shu, S. Study on the thermal performance and wind environment in a residential community. *Int. J. Hydrog. Energy* **2016**, *41*, 15868–15878. [CrossRef]
47. Meng, B.; Loonen, R.C.G.M.; Hensen, J.L.M. Performance variability and implications for yield prediction of rooftop PV systems—Analysis of 246 identical systems. *Appl. Energy* **2022**, *322*, 119550. [CrossRef]
48. Siala, K.; Stich, J. Estimation of the PV potential in ASEAN with a high spatial and temporal resolution. *Renew. Energy* **2016**, *88*, 445–456. [CrossRef]
49. Qu, H.; Du, Z.; Kong, Q. Experimental study on the effect of tilt angle on the output parameters of a photovoltaic-phase change material (PV-PCM) system under wind conditions. *J. Energy Storage* **2024**, *102*, 114263. [CrossRef]
50. Farouk, N.; Babiker, S.; Alqsair, U.F. Boosting electricity generation associated with Saudi Arabi buildings using PCM and PV cells on walls and roof leading to a sustainable building. *Case Stud. Therm. Eng.* **2024**, *64*, 105444. [CrossRef]
51. Luo, Z.; Huang, Z.; Xie, N.; Gao, X.; Xu, T.; Fang, Y.; Zhang, Z. Numerical and experimental study on temperature control of solar panels with form-stable paraffin/expanded graphite composite PCM. *Energy Convers. Manag.* **2017**, *149*, 416–423. [CrossRef]
52. Leng, Z.; Yuan, Y.; Cao, X.; Zeng, C.; Zhong, W.; Gao, B. Heat pipe/phase change material thermal management of Li-ion power battery packs: A numerical study on coupled heat transfer performance. *Energy* **2022**, *240*, 122754. [CrossRef]
53. Kant, K.; Shukla, A.; Sharma, A.; Biwole, P.H. Heat transfer studies of photovoltaic panel coupled with phase change material. *Sol. Energy* **2016**, *140*, 151–161. [CrossRef]
54. Biwole, P.H.; Woloszyn, M.; Pompeo, C. Heat transfers in a double-skin roof ventilated by natural convection in summer time. *Energy Build.* **2008**, *40*, 1487–1497. [CrossRef]
55. Sharples, S.; Charlesworth, P.S. Full-scale measurements of wind-induced: Convective heat transfer from a roof mounted flat plate solar collector. *Sol. Energy* **1998**, *62*, 69–77. [CrossRef]

Disclaimer/Publisher's Note: The statements, opinions and data contained in all publications are solely those of the individual author(s) and contributor(s) and not of MDPI and/or the editor(s). MDPI and/or the editor(s) disclaim responsibility for any injury to people or property resulting from any ideas, methods, instructions or products referred to in the content.